Physical Analysis and Design of Resonant Plasma-Wave Transistors for Terahertz Emitters

Jong Yul Park, *Student Member, IEEE*, Sung-Ho Kim, *Student Member, IEEE*, Sung-Min Hong, *Member, IEEE*, and Kyung Rok Kim, *Member, IEEE*

Abstract—In this work, we performed physical analysis of resonant plasma-wave transistors (PWTs) for terahertz (THz) emitters. Through the analytical decomposition of plasma-waves into upstream and downstream focusing on the different phase velocity, we show that the reflection coefficient is over unity and newly introduce the PWT design window based on a simple 2-D plot, which can provide both the maximum channel length ($L_{\max}$) and operation frequency. By our design window analysis, strained silicon channel with a momentum relaxation time of 50–160 fs (i.e., channel mobility 500–1500 cm²/Vs) show technology-compatible $L_{\max}$ as 12–40 nm with a tunable resonance frequency of 2–10 THz.

Index Terms—Plasma-wave transistor (PWT), terahertz (THz), emitter, design window, maximum channel length, strained silicon, momentum relaxation time, mobility, resonance frequency.

I. INTRODUCTION

SOLID-STATE electronic devices have been considered as one of the most promising platform for miniaturization of terahertz (THz) technology [1], which can give a commercial impact to the various potential industries, such as high data-rate wireless communication, security or food inspection imaging, and bio-medical spectroscopy, while optical devices are based on large foot-print facilities. In order to increase the operation frequency of electronic devices up to THz regime, collective electron density propagation i.e., plasma-mode [2]–[4], where its plasma-wave velocity (s) is 10–100 times faster than local electron drift velocity (v_0) in transit-mode field-effect transistors (FETs), has been in significant attention since it can overcome the cutoff frequency (f_T) limitations from the conventional transit-mode high-speed devices such as heterojunction bipolar transistors (HBTs) [5] or Schottky barrier diodes (SBDs) [6].

The plasma-mode is divided into resonant and non-resonant regime with a criterion of unity quality factor $\omega\tau_p = 1$ [7], [8] where $\omega(= 2\pi f)$ is the angular frequency of plasma-wave and

τ_p is the momentum relaxation time which is linearly proportional to the channel mobility (μ) as $\mu = q\tau_p/m$ where m is the effective mass of 2-D electron gas (2DEG) in the channel of FETs. Therefore, III–V high electron mobility transistors (HEMTs) have been extensively studied for plasma-mode THz emitters [9]–[11] and detectors [12], [13]in resonant regime ($\omega\tau_p > 1$) with a tunable frequency above 1 THz at room temperature. Owing to relatively low mobility in silicon (Si) FETs, only non-resonant detectors with $\omega\tau_p < 1$ have been demonstrated on CMOS technology platform in sub-THz regime (<1 THz) [14]–[17]. Even though CMOS-based plasmonic THz detectors are showing competitive performance with other commercial THz detectors working at room temperature, there has been no experimental report of THz wave emission based on Si CMOS devices, which has great advantages of the low-cost small-size integrated THz systems on a chip with both emitter and detector.

In terms of the theoretical investigations on plasma instability in a diffusive or quasi-ballistic channel, by extending the standard 1-D Dyakonov–Shur theory [2], [3], more generalized approaches for practical boundary conditions have been reported considering the higher-order modes of plasma oscillations in nonuniform channel [18]–[20], hydrodynamic instability in ungated 2-D electron flow [21], [22] and even the transverse distribution of the plasmonic fields around 2-D channel such as mode decomposition technique [23]–[25] and analytical modal solution of Maxwell and hydrodynamic equations [26]. While most of the theoretical analyses for the plasma-wave instability have been performed only by taking III–V HEMTs as an examplary platform and disregarding low-mobility nano-CMOS devices [18]–[28], our previous works, which have been focusing on the fundamental (lowest) mode of plasma-wave resonance in the gated channel, reported the possibility of strained Si (s-Si) plasma-wave transistors (PWTs) with enhanced mobility for THz emitters by defining the maximum channel length ($L_{\max}$) in the unique resonant PWT design window [29], [30].

In this work, we present the advanced physical analysis and design of resonant PWTs for THz emitters by decomposing the downstream and upstream plasma-wave velocity ($s \pm v_0$) in a quasi-ballistic channel where s and v_0 are close enough to compete with each other. These physical investigations provide more accurate analysis and design window of FET-based resonant PWTs with a critical dimension of $L_{\max}$ and operation frequency under the comparable $s \sim v_0$ range on the s-v_0 plot. Details of the physical analysis are described in Section II. The application results of the advanced design window for various channel materials are discussed in Section III.
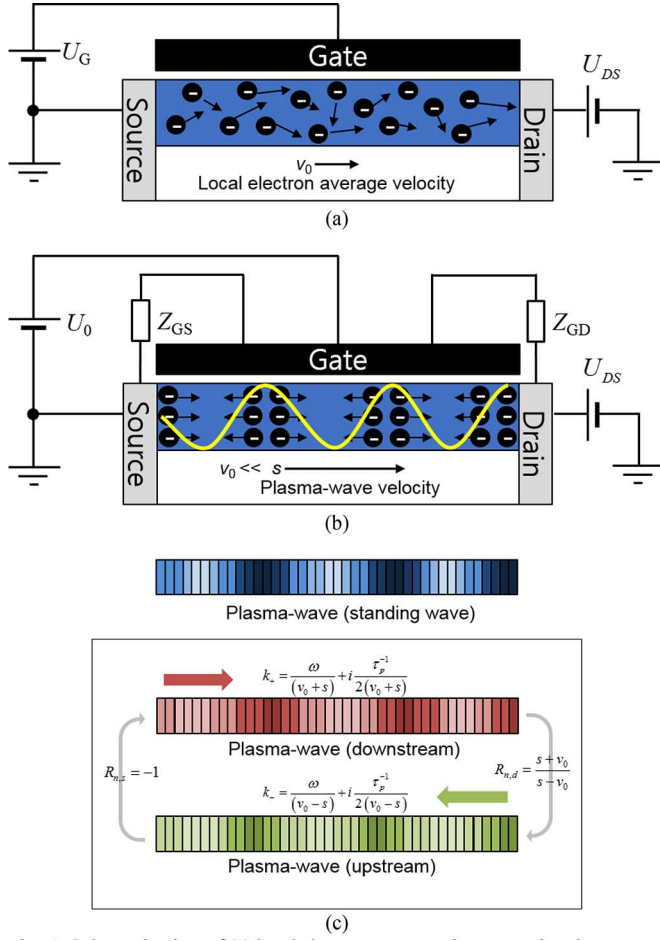
Fig. 1. Schematic view of: (a) local electron transport in conventional FETs and (b) collective electron density (plasma) oscillations in time and space (wave) in PWTs under asymmetric boundary conditions, which is an exemplary case with 11th harmonic ($N = 11$). (c) Top view of PWT channel which shows that spatial distribution of the channel plasma-wave, which consists of downstream and upstream.

II. PHYSICAL ANALYSIS OF PLASMA-WAVE INSTABILITY

Fig. 1(a) schematically illustrates that the key parameter in the conventional FET theory is v_0 to explain local electron drift transport under the finite μ and τ_p. In high density ballistic channel with gate overdrive voltage ($U_0 = U_g - U_{th}$ where U_g is dc gate voltage and U_{th} is threshold voltage), however, the frequent collisions between the local electrons induce the collective behavior of channel 2DEG. As shown in Fig. 1(b), the plasma-wave, which is the oscillation (wave) of the 2DEG density (plasma), can be obtained in the channel of FET (i.e., PWT) under ac short at source (impedance $Z_{GS} = 0$) by dc U_0 and ac open at drain ($Z_{GD} = \infty$) by dc current from standard 1-D Dyakonov–Shur theory [2]. This plasma-wave velocity s is the key parameter of PWT, since it determines the angular frequency $\omega = \omega' + i\omega''$ and its harmonics under given v_0 of FET by following equation as [2], [18]

$$\omega' = \frac{s^2 - v_0^2}{2Ls} N\pi \tag{1}$$

$$\omega'' = \frac{s^2 - v_0^2}{2Ls} \ln\left|\frac{s + v_0}{s - v_0}\right| - \frac{1}{2\tau_p} \tag{2}$$

where L is the channel length and N is an odd integer. Fig. 1(c) illustrates that the plasma-wave forms a standing wave with this frequency of (1) from the superposition of downstream and upstream plasma-waves with different velocity during reflections in the diffusive or quasi-ballistic channel cavity.

For physical and quantitative analysis of this plasma-wave resonance in gated PWT channel, the decomposed analytical model of downstream and upstream in the resonant channel cavity with finite $\mu(\tau_p)$ is now being derived focusing on the fundamental (lowest) mode ($N = 1$). Based on the governing formalism of the hydrodynamic Euler equation and continuity equation with the assumptions of the first-order oscillation terms as n_1, v_1, and U_1 in the plasma-wave $n(x,t) = n_0 + n_1(x,t)$, electron velocity $v(x,t) = v_0 + v_1(x,t)$, and electric potential $U(x,t) = U_0 + U_1(x,t)$, where $n_0 = CU_0/e$ is the surface electron density, C is the areal capacitance of the oxide, e is the elementary electronic charge [2], the analytical solutions of the decomposed downstream and upstream plasma-wave dispersion relation explicitly as

$$k_\pm = \frac{\omega'}{(v_0 \pm s)} + i\frac{\omega''}{(v_0 \pm s)} + i\frac{\tau_p^{-1}}{2(v_0 \pm s)}$$
$$= \alpha_\pm + i\beta_\pm + i\zeta_\pm \tag{3}$$

where k_+ and k_- are the respective wave number of downstream and upstream plasma-wave as illustrated in Fig. 1(c). From (3), the oscillation terms of n_1 can be represented by the linear-independent superposition of n_{1+} and n_{1-} as

$$n_1(x,t) = n_{1+} + n_{1-} = (C_+ e^{ik_+ x} + C_- e^{ik_- x})e^{-i\omega t}$$
$$\text{Re}[n_{1\pm}(x,t)] = C_\pm e^{-(\beta_\pm + \zeta_\pm)x + \omega'' t}$$
$$\times [\cos(\alpha_\pm x)\cos(\omega' t) + \sin(\alpha_\pm x)\sin(\omega' t)] \tag{4}$$

where C_+ and C_- are perturbation coefficients for downstream and upstream, respectively. Likewise, v_1 and U_1 also have perturbation coefficients, which are not clearly defined in their relations and thus, it is hard to obtain the analytical solution for the current density $j(x,t)$ from the simple relation of $j/q = nv$ $= n_0 v_0 + (n_1 v_0 + n_0 v_1)e^{-i\omega t} + n_1 v_1 e^{-2i\omega t}$ with the first-order current flux of $j_1 = (n_1 v_0 + n_0 v_1)e^{-i\omega t}$.

At this point, for the analytical j_1 with more simplified formalism (not by defining v_1 with unknown perturbation coefficients), we use the first order of continuity equation as

$$\frac{\partial n_1}{\partial t} + v_0 \frac{\partial n_1}{\partial x} + n_0 \frac{\partial v_1}{\partial x} = 0 \tag{5}$$

which yields the analytical solution of $n_1 v_0 + n_0 v_1 = (\omega/k)n_1 = j_1$. By this analytical approach, j_1 can be represented in the form of linear-independent downstream and upstream as follows:

$$j_1(x,t) = j_{1+} + j_{1-} = \left(\frac{\omega}{k_+} C_+ e^{ik_+ x} + \frac{\omega}{k_-} C_- e^{ik_- x}\right)e^{-i\omega t} \tag{6}$$

with each phase velocity of $\omega/k_\pm$ which is actually plasma-wave velocity rather than electron drift velocity.
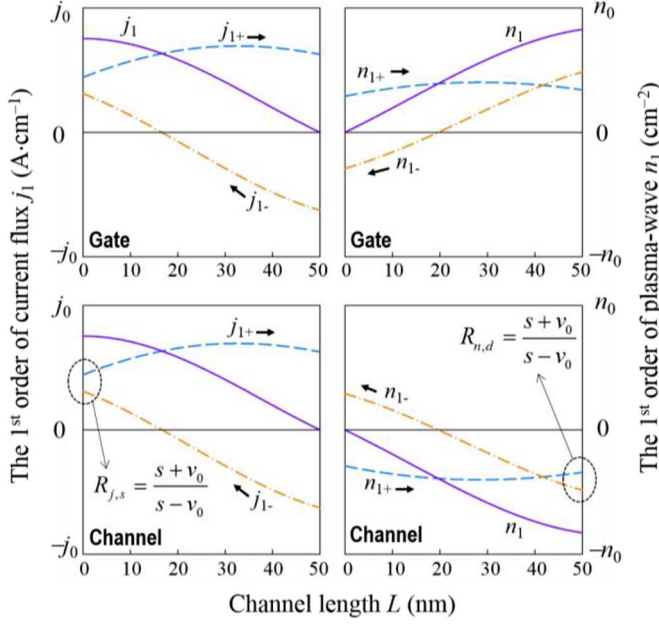
Fig. 2. Calculation results of first harmonic $(N = 1)n_1$ and j_1 after 150 ps in the gate and channel for PWT with $L = 50$ nm, $\tau_p = 100$ fs, $m = 0.028m_0$, $s = 1.5 \times 10^8$ cm/s, and $v_0 = 2.6 \times 10^7$ cm/s. Here $f = 7$ THz, $n_0 = 7.73 \times 10^{12}$ cm^{-2} and $j_0 = 32$ A·cm^{-1} assuming the initial perturbation coefficient $C_+ = -C_- = 2.16 \times 10^5$ cm^{-2}.

As shown in Fig. 2, by using (6) and (4), it is possible to describe the behavior of decomposed plasma-waves $n_{1\pm}(x, t)$ and current fluxes $j_{1\pm}(x, t)$ both in the PWT gate and channel where collision terms $(e^{-\zeta \pm x})$ are included. Actually, there has been vague arguments for reflections of plasma-wave at the boundaries. In [2], Dyakonov and Shur state that the amplitude ratio of the reflected and oncoming waves is $(s + v_0)/(s - v_0)$ without using the exact terminology of reflection coefficient. In the subsequent investigation by Crowne [18], the reflection coefficient $(v_0 - s)/(v_0 + s)$ is always lower than unity in absolute value for $0 < v_0 < s$. On the one hand, the current and voltage reflection coefficient for the Dyakonov–Shur instability has been investigated by Cheremisin et al.[20] in the form of equation. In this work, we performed the physical analysis for the reason why the reflection coefficient is larger than unity by taking the analogy with the transmission line model between gate and channel. This analogy itself has been mentioned in Dyakonov–Shur theory [2]. But, our present work is distinguished in that we take this analogy to investigate the reason why reflection coefficient >1 as illustrated in Fig. 2.

It can be noted that the relation between plasma-wave and current flux is similar to voltage and current waves in the transmission line theory. Firstly, let us suppose that the j_{1+} (downstream) moves toward drain side in the channel (lower-left one of Fig. 2). Due to ac open condition on drain side ($Z_{GD} = \infty$ at $x = L$), the j_{1+} reflects with $-180°$ of phase difference in order to make $j_1(x = L) = 0$ so that the reflection coefficient of j_1 at the drain side is $R_{j,d} = -1$. The n_{1+} (downstream) at the drain side is also reflected and changes to n_{1-} (upstream) in the channel (Fig. 2, lower right). At this reflection of n_1, the n_{1+} has the same phase with the n_{1-} because the number of

electrons should increase at the drain side by the addition of the electrons in the reflected j_{1-} (upstream) in the channel. By the boundary condition of $j_1(L) = 0$ from (6), the reflection coefficient $(R_{n,d})$ for the n_1 at the drain side can be obtained from (4) as

$$R_{n,d} = \frac{n_{1-}(L)}{n_{1+}(L)} = \frac{k_+}{k_-} = \frac{s + v_0}{s - v_0}. \qquad (7)$$

Subsequently, the upstream n_{1-} and j_{1-} move toward the source side in the channel and transfer to the gate region (upper ones of Fig. 2) because the channel and gate are connected with ac short condition at the source ($x = 0$). Thus, the j_{1-} from the gate region also flows to the channel and changes to j_{1+} with increased plasma-wave velocity, which has the same phase to the j_{1-} in the channel. Therefore, it seems that the j_{1-} just reflects and changes to the j_{1+} so that the reflection coefficient $(R_{j,s})$ of j_1 at the source side can be calculated by each component of $j_{1+}(0)$ and $j_{1-}(0)$ using (6)

$$R_{j,s} = \frac{j_{1+}(0)}{j_{1-}(0)} = \frac{k_+}{k_-} = \frac{s + v_0}{s - v_0}. \qquad (8)$$

At the source with ac short condition ($Z_{GS} = 0$ at $x = 0$), the n_1 is zero because the phase of transferred n_{1+} from the gate is opposite to the n_{1-} in the channel, i.e., the reflection coefficient of n_1 at the source is $R_{n,s} = -1$. The results of (7) and (8) mean that $R_{n,d}$ and $R_{j,s}$ are always larger than unity when U_{DS} is biased while they become unity without U_{DS}, which is the same results for the standing wave in the transmission line theory with the same boundary conditions and ac voltage source [31].

The sum of j_{1+} and j_{1-} makes standing wave (j_1) which has anti-node and node at the source and drain side, respectively, while the sum of n_{1+} and n_{1-} also forms standing wave (n_1) which has node and anti-node at the source and drain side, respectively. It should be noted that the resonance of PWTs originates from these standing waves with the growth of the amplitude during multiple reflections. Since the n_1 in the channel and gate have different phase with $-180°$, the electric dipole is formed and oscillates in the PWT so that the electromagnetic (EM) wave is emitted with THz frequency.

Based on this physical analysis of the plasma-wave in the channel, Fig. 3 describes that the quality of plasma-wave resonance is determined by the condition of $(s - v_0)\tau_p/L$. In terms of resonance, the ideal case is that standing wave has fixed node and anti-node so that the simple harmonic oscillator is formed. In the PWT channel, however, the oscillation of plasma-wave rather shows the behavior of coupled harmonic oscillator, which distributes the energy to make intended frequency and intensity of EM wave, as illustrated at points in $2T/5$ and $4T/5$ in Fig. 3.

In comparable $s \sim v_0$ range, the condition of $(s - v_0)\tau_p/L$ can be a criterion to judge how standing wave is close to the simple harmonic oscillator. As the velocity of upstream is decreased by increasing v_0 or decreasing s, which means that $(s - v_0)\tau_p/L$ is lowered and $R_{n,d}$ is increased, the quality of resonance becomes worse as shown in Fig. 3 because the simple harmonic oscillator gradually changes to the coupled harmonic oscillator as the velocity difference between downstream and upstream increase.
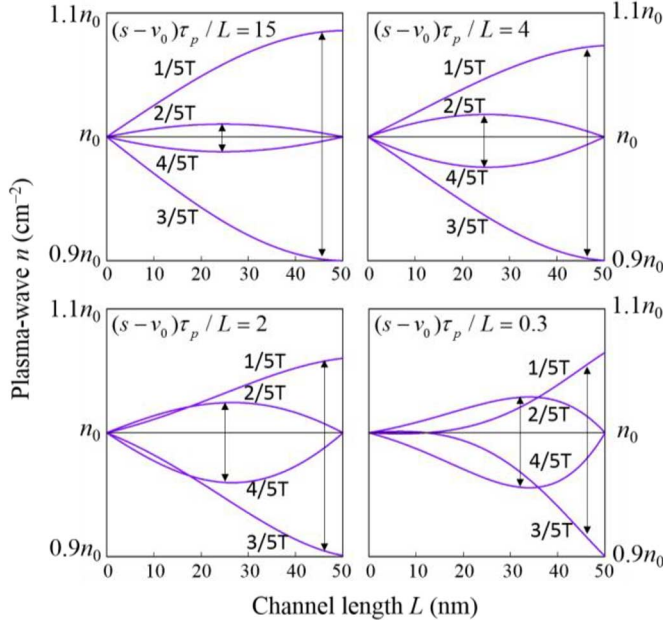
Fig. 3. Calculated waveforms of first harmonic plasma-wave $n(=n_0 + n_1)$ in the channel of the same PWT in Fig. 2 for $s = 7.70 \times 10^8, 2.25 \times 10^8, 1.25 \times 10^8$ and 4.00×10^7 cm/s, respectively. in each plot. Harmonic waveforms with different period (T) are plotted at each same periodic time of $T/5, 2T/5, 3T/5$, and $4T/5$.

III. RESONANT PWT DESIGN FOR THZ EMITTERS

For the physical evaluation of resonant PWT THz Emitters, the design window of 2-D s-v_0 plot, which has two independent variables of s from plasma-wave theory and v_0 from FET theory in each axis, should be introduced since those of s and v_0 in comparable range determine the desired operation frequency of PWT with given L as shown in (1). On this s-v_0 plot, the resonance window can be confined by physical conditions in Table I once L and the channel material with $\mu(m, \tau_p)$ of PWT are properly assumed. For example, as shown in Fig. 4, by assuming $m = 0.028m_0$ and $\mu = 6300$ cm$^2 \cdot$V$^{-1} \cdot$s^{-1} (i.e., $\tau_p = 100$ fs), the resonance window provides the operation ranges of PWT THz emitter with $L = 50$ nm, which are $7.74 \times 10^7 < s < 2.05 \times 10^8$ cm/s and $2.72 \times 10^7 < v_0 < v_{\text{inj}} = 3.22 \times 10^7$ cm/s at room temperature in the operation frequency range $3.4 < f < 10$ THz.

In terms of the advanced feature compared to our previous work [29], the reflection condition of $(s - v_0)\tau_p/L > 1$, as explained in Section II, is newly considered on the s-v_0 plot by the following straight line equation as

$$s = v_0 + \frac{L}{\tau_p} \quad (9)$$

Most of the previous theoretical works have considered only the extreme case of $s \gg v_0$ i.e., constant line of $s = L/\tau_p$ which can be effective to the resonance window by being drawn above the underdamped condition of $\omega'\tau_p = 1$ i.e., $s = (2/\pi)L/\tau_p$ only at the very small v_0 region. In the comparable $s \sim v_0$ range, however, the reflection condition of (9) should be considered for more accurate evaluation of PWT THz emitter with a quasi-ballistic channel since (9) with unity slope is placed on the s-v_0
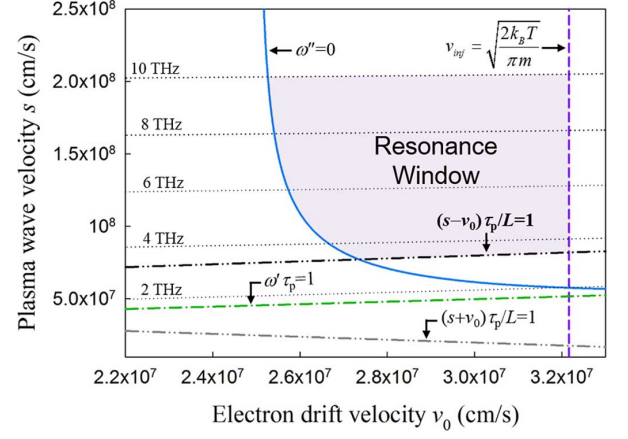

Fig. 4. Resonance window for PWT with $L = 50$ nm and $\tau_p = 100$ fs by applying the reflection condition of $(s - v_0)\tau_p/L > 1$, which result in the reduction of tunable operation frequency range. Every point in this $s - v_0$ plot can be represented by Mach number $M = v_0/s$.

TABLE I
PHYSICAL CONDITIONS FOR RESONANT PWT THZ EMITTERS

Physical Condition for Plasma-wave	Criteria
Underdamped	$\omega\tau_p > 1$
Reflection	$(s-v_0)\tau_p/L > 1$
Instability	$v_0 < v_{\text{inj}} < s$
Increment	$\omega'' > 0$
Frequency	$f < 10$ THz

plot always above $\omega'\tau_p = 1$ from (1) by instability condition with Mach number $M = v_0/s < 1$, as shown in Fig. 4.

To apply (9) onto the s-v_0 plot, the proper estimation of possible L, which is the critical dimension of PWT design, should be performed based on the maximum channel length $(L_{\max})$ as defined by

$$L_{\max} = \frac{s_{\max}|1 - M_{\min}^2|}{4 \times 10^{13}} \quad (10)$$

where $M_{\min} = \{\exp[4\tau_p \times 10^{13}] - 1\}/\{\exp[4\tau_p \times 10^{13}] + 1\}$ and $s_{\max} = v_{\text{inj}}/M_{\min}$ [29]. Fig. 5 illustrates that the resonance windows become reduced with same $M_{\min}$ as L increases and $L_{\max}$ is determined at the resonance point of $v_0 = v_{\text{inj}}$ and $s = s_{\max}$ for 10 THz, which is the maximum frequency of so-called "THz gap". It should be noted that this arbitrarily assumed PWT with $\tau_p = 100$ fs and $m = 0.028m_0$ can be operated as the THz emitters only when the channel length is below $L_{\max} = 64$ nm. Based on this concept of $L_{\max}$, we can evaluate possible $L < L_{\max}$ from experiments of FETs with τ_p and m for THz emitter operation.

The calculation results of $L_{\max}$ are summarized in Table II for Si-compatible (Si, Ge, and strained Si) or compound semiconductor (InAs, GaAs, and InGaAs) channel materials in MOSFET [32]–[37] and HEMT structures [38]–[40]. As listed in Table II, HEMT structure shows higher channel mobility than MOSFET on the same material due to the suppression of surface roughness scattering. In case of InGaAs HEMTs [38], [39], $L_{\max}$ ranges around 170 nm on average which can explain the experimental data of 2.9 THz emission from 130-nm InGaAs HEMT [41]. Focusing on the s-Si channel MOSFET
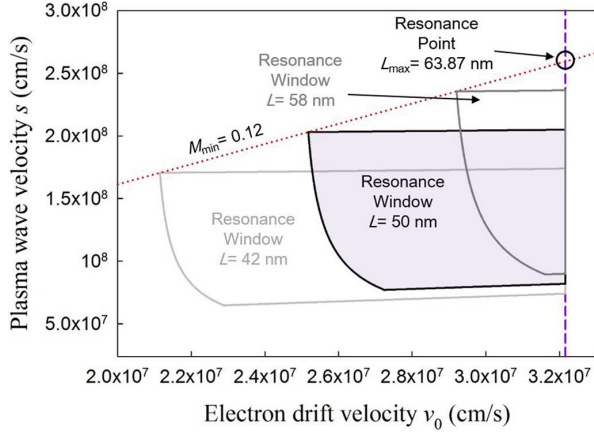
Fig. 5. Resonance windows of PWT with $\tau_p = 100$ fs for $L = 42, 50,$ and 58 nm. Each resonance window has the same $M_{\min}$ and $L_{\max}$ is determined as 64 nm at the point of $v_0 = v_{\mathrm{inj}}$ and $s = s_{\max}$ for 10 THz.

TABLE II
CALCULATION RESULTS OF $L_{\max}$ FOR VARIOUS CHANNEL MATERIALS IN MOSFET AND HEMT STRUCTURES

Material [MOSFET]	μ (cm²/Vs)	m/m_0	$L_{\max}$ (nm)
InAs	10500 [32]	0.023	96.94
In$_{0.53}$Ga$_{0.47}$As	6600 [33]	0.045	85.40
GaAs	4500 [34]	0.063	68.87
Ge	1100 [35]	0.12	22.90
strained Si (s-Si)	500 [36]	0.19	12.87
Si	250 [37]	0.26	7.24
Material [HEMT]	**μ (cm²/Vs)**	**m/m_0**	**$L_{\max}$ (nm)**
InAs	13000 [38]	0.023	120.26
In$_{0.53}$Ga$_{0.47}$As	9500 [38]	0.045	123.15
	16500 [39]	0.045	214.15
strained Si (s-Si)	1500 [40]	0.19	39.87
	1000 [40]	0.19	26.45

[37] and n-type modulation-doped FET (n-MODFET) [40] where $L_{\max}$ increases up to 40 nm, resonant PWT operation for THz emitters can be expected with a current deca–nanoscale Si CMOS technology.

For a relative comparison of the expected resonance windows from Si-compatible PWTs with deca-nanoscale L below $L_{\max}$, the channel length of L can be assigned to the additional z-axis based on the 2-D s-v_0 plot. Fig. 6 describes the 3-D plot of resonance windows for PWTs based on Si-compatible channel under each given L of 6, 10, 14, 18, 22, and 26 nm (z-axis). According to the enhancement of channel mobility, relatively larger resonance window can be obtained only if given $L < L_{\max}$. In case of $L = 26$ nm, s-Si n-MODFET (one of the HEMTs) with $\mu = 1500$ cm²·V⁻¹·s⁻¹ only exhibits the possible resonance window having a wide operation frequency range of 2.1 THz $< f <$ 10 THz. Based on the lighter effective mass assumption of s-Si as $m = 0.19m_0$, the boundary of v_{inj} a little bit more increased than Si channel ($m = 0.26m_0$) as shown in the case of $L = 6$ nm where conventional Si MOSFETs with $\mu = 250$ cm²·V⁻¹·s⁻¹ exhibit very challenging resonance window.

It is noticeable that, as the channel mobility improved, the resonance window is broaden in the lower left direction at the same channel length as shown in Fig. 7, which illustrates the resonant windows for s-Si PWTs at $L = 10$ nm. Qualitatively,
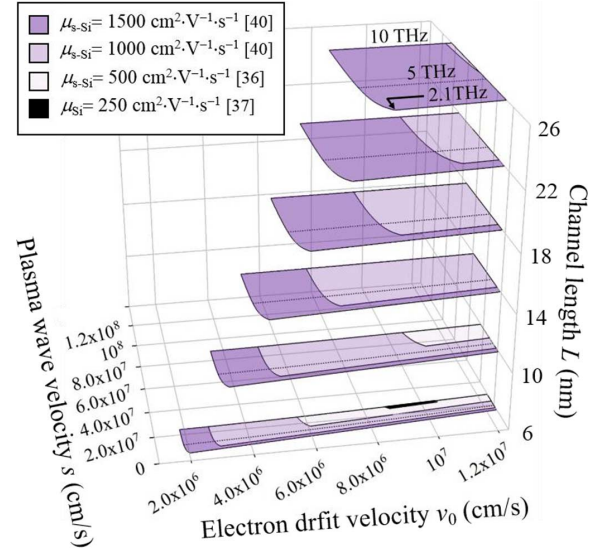

Fig. 6. Resonance window for Si and strained-Si channel on 3-D plot by assigning L to z-axis. The minimum operation frequency range for the $\mu_{s-Si} = 1500$ cm²·V⁻¹·s⁻¹ is near 2.1 THz at $L = 26$ nm, where the reflection condition $(s - v_0)\tau_p/L$ contributes to form boundary of resonant window.
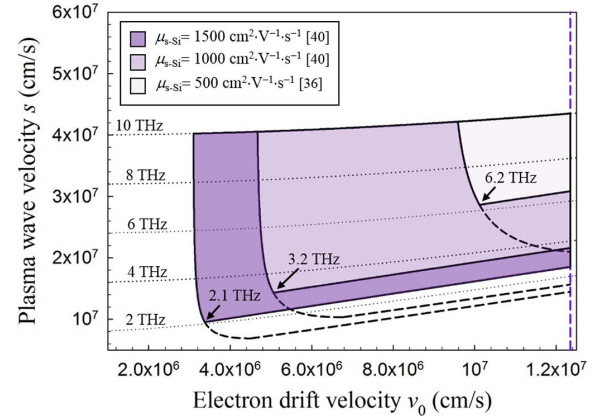

Fig. 7. 2-D design window for PWT THz emitter based on s-Si MOSFET and HEMT structures at $L = 10$ nm.

enhanced mobility i.e., increased τ_p of PWT channel guarantees more underdamped, reflection and increment of plasma-waves, which means that rare scattering events sustain its amplitude and propagation distance further so that the resonance occurs with lower v_0 and s at fixed L. For quantitative results, in s-Si HEMT with $\mu = 1500$ cm²·V⁻¹·s⁻¹ and $L = 10$ nm, the resonant PWT can be achieved within the operation range of $9.55 \times 10^6 < s < 4.35 \times 10^7$ cm/s and $3.10 \times 10^6 < v_0 < 1.23 \times 10^7$ cm/s in the operation frequency of $2.1 < f < 10$ THz, which is broader than s-Si MOSFET with $\mu = 500$ cm² · V⁻¹·s⁻¹ case $(2.87 \times 10^7 < s < 4.35 \times 10^7$ cm/s and $9.59 \times 10^6 < v_0 < 1.23 \times 10^7$ cm/s in the operation frequency range of $6.2 < f < 10$ THz). The dashed lines in Fig. 7 are boundaries by only considering increment ($\omega'' > 0$) and underdamped ($\omega'\tau_p > 1$) condition without the reflection condition ($(s - v_0)\tau_p/L > 1$). When the PWT channels become more diffusive and $s \sim v_0$ ranges are comparable, the $(s - v_0)\tau_p/L > 1$ condition should be included for more realistic and accurate design of PWT THz emitters since the operation frequency range is modulated.

IV. CONCLUSION

Physical analysis of resonant PWTs has been performed by analytical modeling of channel plasma-waves for THz emitters. Based on the decomposed analytical solutions of each upstream and downstream plasma-wave in the diffusive or quasi-ballistic channel, the reflection coefficient over unity at boundaries has been proved and the advanced PWT design window of a simple 2-D plot has been introduced. By using our resonance window analysis of PWTs from experimental data, it can be expected that strained Si PWTs with enhanced mobility show the current Si CMOS technology-compatible $L_{\max}$ range as 12–40 nm with a tunable resonance frequency of 2–10 THz for THz emitters.

REFERENCES

[1] *Terahertz Sensing Technology, Volume I. Electronic Devices & Advanced Technology*, D. Woolard, W. Loerop, and M. S. Shur, Eds.. Singapore: World Scientific, 2003.

[2] M. Dyakonov and M. Shur, "Shallow water analogy for a ballistic field effect transistor: New mechanism of plasma wave generation by dc current," *Phys. Rev. Lett.*, vol. 71, no. 15, pp. 2465–2468, Oct. 1993.

[3] M. I. Dyakonov and M. S. Shur, "Plasma wave electronics: Novel terahertz devices using two dimensional electron fluid," *IEEE Trans. Electron Devices*, vol. 43, no. 10, pp. 1640–1645, Oct. 1996.

[4] V. Ryzhii and M. S. Shur, "Plasma wave electronics devices," in *Proc. ISDRS*, 2003, p. 200.

[5] Y. Zhao, E. Öjefors, K. Aufinger, T. F. Meister, and U. R. Pfeiffer, "A 160-GHz subharmonic transmitter and receiver chipset in an SiGe HBT technology," *IEEE Trans. Microw. Theory Techn.*, vol. 60, no. 10, pp. 3286–3299, Oct. 2012.

[6] R. Han *et al.*, "Active terahertz imaging using schottky diodes in CMOS: Array and 860-GHz pixel," *IEEE J. Solid-State Circuits*, vol. 48, no. 10, pp. 2296–2308, Oct. 2013.

[7] M. I. Dyakonov, "Generation and detection of Terahertz radiation by field effect transistors," *Comptes Rendus Physique*, vol. 11, pp. 413–422, 2010.

[8] W. Knap and M. I. Dyakonov, "Filed effect transistors for terahertz application," in *Handbook of Terahertz Technology for Imaging, Sensing and Communications*. Amsterdam, the Netherlands: Elsevier, 2013, ch. 5, pp. 121–155.

[9] W. Knap *et al.*, "Terahertz emission by plasma waves in 60 nm gate high electron mobility transistors," *Appl. Phys. Lett.*, vol. 84, no. 13, pp. 2331–2333, Mar. 2004.

[10] S. Boubanga-Tombet *et al.*, "Room temperature coherent and voltage tunable terahertz emission from nanometer-sized field effect transistors," *Appl. Phys. Lett.*, vol. 97, 2010, Art. ID 262108.

[11] T. Otsuji, T. Komori, T. Watanabe, T. Suemitsu, D. Coquillat, and W. Knap, "Plasmon-resonant microchip emitters and detectors for terahertz sensing and spectroscopic applications," in *Proc. SPIE*, 2010, vol. 7671, pp. 767102-1–767102-12.

[12] J.-Q. Lü, M. S. Shur, J. L. Hesler, L. Sun, and R. Weikle, "Terahertz detector utilizing two-dimensional electronic fluid," *IEEE Electron Devices Lett.*, vol. 19, no. 10, pp. 373–375, Oct. 1998.

[13] J. Mateos and T. Gonzalez, "Plasma enhanced terahertz rectification and noise in InGaAs HEMTs," *IEEE Trans. THz Sci. Technol.*, vol. 2, no. 5, pp. 562–569, Sep. 2012.

[14] W. Knap *et al.*, "Plasma wave detection of sub-terahertz and terahertz radiation by silicon field-effect transistors," *Appl. Phys. Lett.*, vol. 85, no. 4, pp. 675–677, Jul. 2004.

[15] E. Öjefors, U. R. Pfeiffer, A. Lisauskas, and H. G. Roskos, "A 0.65 THz focal-plane array in a quarter-micron CMOS process technology," *IEEE J. Solid-State Circuits*, vol. 44, no. 7, pp. 1968–1976, July 2009.

[16] F. Schuster *et al.*, "Broadband terahertz imaging with highly sensitive silicon CMOS detectors," *Opt. Express*, vol. 19, no. 8, pp. 7827–7832, Apr. 2011.

[17] A. Gutin, S. Nahar, M. Hella, and M. Shur, "Modeling terahertz plasmonic Si FETs with SPICE," *IEEE Trans. THz Sci. Technol.*, vol. 3, no. 4, pp. 545–549, Sept. 2013.

[18] F. J. Crowne, "Contact boundary conditions and the Dyakonov-Shur instability in high electron mobility transistors," *J. Appl. Phys.*, vol. 82, no. 3, pp. 1242–1254, Aug. 1997.

[19] F. J. Crowne, "Dyakonov-Shur plasma excitations in the channel of a real high electron mobility transistor," *J. Appl. Phys.*, vol. 87, no. 11, pp. 8056–8063, June 2000.

[20] M. V. Cheremisin, M. I. Dyakonov, M. S. Shur, and G. Samsonidze, "Influence of electron scattering on current instability in field effect transistors," *Solid-State Electron.*, vol. 42, no. 9, pp. 1737–1742, 1998.

[21] M. V. Cheremisin and G. G. Samsonidze, "Current instability and single-mode THz generation in ungated two-dimensional electron gas," *Solid-State Electron.: Short Commun.*, vol. 52, pp. 338–340, 2008.

[22] W. R. Calderon-Munoz, D. Jena, and M. Sen, "Hydrodynamic instability of confined two-dimensional electron flow in semiconductors," *J. Appl. Phys.*, vol. 106, pp. 014506-1–0140506-10, 2009.

[23] O. Sydoruk, R. R. A. Syms, and L. Solymar, "Amplifying mirrors for terahertz plasmons," *J. Appl. Phys.*, vol. 112, pp. 104512-1–104512-10, 2012.

[24] O. Sydoruk, "Drifting plasmons in open two-dimensional channels: Modal analysis," *J. Phys. D: Appl. Phys.*, vol. 46, pp. 135103-1–135103-8, 2013.

[25] O. Sydoruk, "Amplification of drifting semiconductor plasmons and effects of carrier collisions and diffusion," *J. Phys. D: Appl. Phys.*, vol. 46, pp. 345101-1–345101-7, 2013.

[26] M. A. Khorrami, S. E.-Ghazaly, S.-Q. Yu, and H. Naseem, "Terahertz plasmon amplification using two-dimensional electron-gas layers," *J. Appl. Phys.*, vol. 111, pp. 094501-1–094501-6, 2012.

[27] M. Dyakonov and M. Shur, "Detection, mixing, and frequency multiplication of terahertz radiation by two-dimensional electronic fluid," *IEEE Trans. Electron. Devices*, vol. 43, no. 3, pp. 380–387, Mar. 1996.

[28] M. S. Shur and J.-Q. Lü, "Terahertz sources and detectors using two-dimensional electronic fluid in high electron-mobility transistors," *IEEE Trans. Microw. Theory Techn.*, vol. 48, no. 4, pp. 750–756, Apr. 2000.

[29] J. Y. Park, S.-H. Kim, Y.-K. Choi, S. Hong, S.-G. Lee, and K. R. Kim, "Possibility and design of resonant terahertz emitters based on nanoscale strained silicon plasma wave transistors with enhanced mobility," *Jpn. J. Appl. Phys.*, vol. 53, 2014, Art. ID 06JE08.

[30] J. Y. Park, S.-H. Kim, and K. R. Kim, "Deca-nanoscale maximum gate length of plasma wave transistor for operating terahertz emitter based on strained silicon platform," in *Proc. 14th IEEE NANO*, Aug. 2014, pp. 150–153.

[31] Jr. B. W. Griffith, "Transmission lines," in *Radio-Electronic Transmission Fundamentals*, 2nd ed. Stevenage, U.K.: SciTech Publishing, 2000, ch. 2, pp. 210–212.

[32] H.-C. Ho, T.-W. Fan, and H.-K. Lin, "Low output-conductance InAs-channel metal-oxide-semiconductor field-effect transistors with SiO_2 gate dielectrics," *Electrochem. Solid-State Lett.*, vol. 14, no. 8, pp. H340–H342, May 2011.

[33] S. J. Bentley *et al.*, "Electron mobility in surface and buried channel flatband $In_{0.53}Ga_{0.47}As$ MOSFETs with ALD Al_2O_3 gate dielectric," *IEEE Electron Device Lett.*, vol. 32, no. 4, pp. 494–496, Apr. 2011.

[34] K. Rajagopalan, J. Abrokwah, R. Droopad, and M. Passlack, "Enhancement-mode GaAs n-channel MOSFET," *IEEE Electron Device Lett.*, vol. 27, no. 12, pp. 959–962, Dec. 2006.

[35] K. Morii, T. Iwasaki, R. Nakane, M. Takenaka, and S. Takaki, "High-performance GeO_2/Ge nMOSFETs with source/drain junctions formed by gas-phase doping," *IEEE Electron Device Lett.*, vol. 31, no. 10, pp. 1092–1094, Oct. 2010.

[36] W. Xiong, C. R. Cleavelin, P. Kohli, C. Huffman, T. Schulz, K. Schruefer, G. Gebara, K. Mathews, P. Patruno, Y. M. L. Vaillant, I. Cayrefourcq, M. Kennard, K. Shin, and T. J. K. Liu, "Impact of strained silicon-on-insulator (sSOI) substrate on FinFET mobility," *IEEE Electron Device Lett.*, vol. 27, no. 7, pp. 612–614, July 2006.

[37] S. Takagi, A. Toriumi, M. Iwase, and H. Tango, "On the universality of inversion layer mobility in Si MOSFET's: Part II—Effects of surface orientation," *IEEE Trans. Electron Devices*, vol. 41, no. 12, pp. 2363–2368, Dec. 1994.

[38] J. A. del Alamo, "Nanometre-scale electronics with III-V compound semiconductors," *Nature*, vol. 479, pp. 317–323, Nov. 2011.

[39] T. Akazaki, J. Nitta, H. Takayanagi, T. Enoki, and K. Arai, "Improving the mobility of an $In_{0.52}Al_{0.48}As/In_{0.53}Ga_{0.47}As$ inverted modulation-doped structure by inserting a strained InAs quantum well," *Appl. Phys. Lett.*, vol. 65, pp. 1263–1265, Sept. 1994.

[40] F. Schäffler, "High-mobility Si and Ge structures," *Semicond. Sci. Technol.*, vol. 12, pp. 1515–1549, Aug. 1997.

[41] M. Hanabe, T. Otsuji, T. Ishibashi, T. Uno, and V. Ryzhii, "Modulation effects of photocarriers on the terahertz plasma-wave resonance in high-electron-mobility transistors under interband photoexcitation," *Jpn, J. Appl. Phys.*, vol. 44, no. 6A, pp. 3842–3847, Jun. 2005.

Jong Yul Park was born in Korea in 1987. He received the B.S. degree with a double major in physics and management from Sejong University, Seoul, Korea, 2013, and is currently working toward the Ph.D. degree in electrical engineering from the School of Electrical Engineering, Ulsan National Institute of Science and Technology, Ulsan, Korea.

His research interests include theoretical framework and analytical simulation of THz electromagnetic wave from plasma-wave transistor (PWT) based on FET structure.

Sung-Ho Kim was born in Korea in 1991. He received the B.S. degree in electrical and computer engineering degree in the School of Electrical and Computer Engineering from Ulsan National Institute of Science and Technology, Ulsan, Korea, in 2014, and is currently working toward Ph.D. degree in electrical engineering from the School of Electrical Engineering, Ulsan National Institute of Science and Technology, Ulsan, Korea.

His research interests include nano-CMOS and THz devices based on plasma wave.

Sung-Min Hong (M'08) was born in Korea in 1978. He received the B.S. degree in electrical engineering and the Ph.D. degree in electrical engineering and computer science from Seoul National University, Seoul, Korea, in 2001 and 2007, respectively.

From 2007 to 2011, he was a Postdoctoral Research Associate with the Institute for Microelectronics and Circuit Theory, Bundeswehr University, Neubiberg, Germany. From 2011 to 2013, he was a Staff Engineer with the Device Laboratory, Samsung Information Systems America (later Samsung Semiconductor Inc.), San Jose, CA. He is currently an Assistant Professor with the School of Information and Communications, Gwangju Institute of Science and Technology, Gwangju, Korea. His current research interests include deterministic Boltzmann equation solvers and simulation of terahertz devices.

Kyung Rok Kim (M'10) was born in Korea in 1976. He received the B.S., M.S., and Ph.D. degrees in electrical engineering from the Department of Electrical Engineering and Computer Science, Seoul National University, Seoul, Korea, in 1999, 2001, and 2004, respectively.

He is currently an Associate Professor with the School of Electrical and Computer Engineering, Ulsan National Institute of Science and Technology (UNIST), Ulsan, Korea. From 2004 to 2006, he was with the Stanford Technology Computer-Aided Design (TCAD) Group of the Center for Integrated Systems, Stanford University, Stanford, CA, where he developed a TCAD based quantum tunneling model, as a Postdoctoral Research Associate. From 2006 to 2010, he was with Samsung Electronics Corporation, Ltd., Suwon-si, Korea, where he developed unified process-device-circuit analysis tools for memory and logic devices, as a Senior Engineer. His current research interests include nanoelectronic emerging devices and circuits, future CMOS and memory devices, low-power nanoscale ICs, and Si quantum-effect devices, neuromorphic devices and circuits, terahertz (THz) detector system, THz plasma-wave devices, and its physical modeling based on the TCAD platform.

Dr. Kim is a member of the IEEE Electron Device Society, a Member of the Institute of Electronics Engineers of Korea (IEEK), and a Member of the Institute of Electronics, Information and Communication Engineers (IEICE).